Brodogradnja/Shipbuilding Volume 65 Number 2, 2014

Xujian Lyu
Hui Tang
Jianglong Sun
Xiaoguang Wu
Xianwen Chen

ISSN 0007-215X
eISSN 1845-5859

SIMULATION OF MICROBUBBLE RESISTANCE REDUCTION ON A SUBOFF MODEL

UDC 629.5(018)
Original scientific paper

Summary

This paper presents a mixture-model based computational fluid dynamics (CFD) simulation on the two-phase microbubble flow over the hull of a SUBOFF model, aimed at assessing the roles of air-injection-to-freestream velocity ratio and air volume fraction in microbubble resistance reduction. The numerical framework consists of the Reynolds-average Navier-Stokes (RANS) equations and the standard $k-\varepsilon$ turbulence model with standard wall function treatment, which is validated, without microbubbles, by existing experimental data of the same SUBOFF model. The effect of velocity ratio is then investigated by comparing different types of the resistance reduction at various water speeds, and the effect of air volume fraction on the friction resistance reduction is also studied with various air injection velocities. This study confirms that both the velocity ratio and air volume fraction play important roles in the microbubble resistance reduction phenomenon.

Key words: Microbubbles; resistance reduction; SUBOFF; CFD;

1. Introduction

The pursuit of higher speeds in water has resulted in many vehicle performance enhancement techniques. One of them is the introduction of an air film along vehicles to reduce skin friction drag. Although reducing hull drag by air injection has been proposed for many years, it still remains under exploited [1-6].

Latorre [7] briefly reviewed the application of bottom air film, as well as towing tank and trial results. The extent of the performance improvement was illustrated in plots of power versus speed. The results of systematic barge model and full-scale tests were used to reveal the influence of air injection on the frictional resistance. It was shown that while the air injection equipment added appendage drag to the barge hull, the bottom airflow resulted in a net drag reduction of 15-18% in model tests and of 10-12% in full scale tests. The drag reduction by the injection of microbubbles into a turbulent boundary layer was investigated using an Eulerian two-fluid model by Mohanarangam et al. [8]. The simulated results were

compared against the experimental findings by Madavan et al. [9]. The complex drag reduction mechanism was examined and explained in context to their numerical results. Special attentions were paid to the effect of bubble coalescence and break-up caused by random collision and turbulence impact. Good agreements against experimental data were obtained in terms of the skin-friction coefficients throughout various air injection rates.

For low- and medium-speed displacement vehicles, the most important component of resistance is the frictional resistance. By reducing the frictional resistance, the total resistance and fuel costs can be decreased significantly. The effect of air lubrication on the resistance of an underwater vehicle was numerically investigated by Doğrul et al. [10]. The analyses were performed by a commercial computational fluid dynamics (CFD) code. For their air lubricated case, the coefficient of frictional resistance was calculated and compared with those of ITTC'57 as well as the case without air lubrication. Skudarnov & Lin [11] used a two-dimensional single-phase CFD model of microbubble-laden flow over a flat plate to assess the role of mixture density variation in microbubble drag reduction. The model consisted of the Reynolds-averaged Navier–Stokes (RANS) equations, the standard k–ω turbulence model, and a convection–diffusion species transport model. Performance of the model was validated with existing experimental data and simulation results of more advanced multiphase two-fluid models.

Ceccio [12] discussed the current existing applications of microbubble techniques on underwater vehicles, and presented the underlying principles and recent advances of the technology. Injection of air leads to the creation of a bubbly mixture near the vehicle surface that significantly modifies the flow within the turbulent boundary layer. There had been significant advances in the understanding of the underlying physical process of drag reduction. The skin friction of the turbulent boundary layer in liquid flows may be reduced when bubbles are present near the vehicle surface. Sanders et al. [13] presented some results at the Reynolds number as high as 210 million from skin-friction drag-reduction experiments for a flat plate. Skin-friction drag reduction was lost when the near-wall shear induced the bubbles to migrate from the plate surface. This bubble-migration phenomenon limited the persistence of bubble-induced skin-friction drag reduction to only the first few meters downstream of the air injector in the experiments.

In this paper the roles of the air-injection-to-freestream velocity ratio and air volume fraction in microbubble drag reduction are assessed via the mixture model based CFD simulations of microbubble injection flow over the hull of a SUBOFF model at high Reynolds numbers. The following sections give detailed description of the numerical framework and its validation. The results of a parametric study on the effects of velocity ratio and air volume fraction on drag reduction are presented and discussed.

2. Numerical framework

The microbubble flow is a two-phase flow consisting of microbubbles and water. Water is a continuous flow, while the microbubbles are a dispersed flow. This two-phase flow system can be treated as a single-phase mixture flow, which is able to reduce resistance by changing the structure of turbulence boundary layer near the hull. The present numerical framework consisted of the Reynolds-average Navier-Stokes (RANS) equations and the standard $k-\varepsilon$ turbulence model with standard wall function treatment. The mixture Eulerian model is used to obtain the velocity and pressure distribution by solving the continuity, momentum, and turbulence equations.

The continuity equation:

$$\frac{\partial u_i}{\partial x_i} = 0 \tag{1}$$

The momentum equation (Reynolds-averaged Navier-Stokes equation):

$$\frac{\partial}{\partial t}(\rho u_i) + \frac{\partial}{\partial x_i}(\rho u_i u_j) = \frac{\partial}{\partial x_j}\left[\mu\left(\frac{\partial u_i}{\partial x_j} + \frac{\partial u_j}{\partial x_i}\right) - \frac{2}{3}\mu\frac{\partial u_i}{\partial x_j}\right] - \frac{\partial P}{\partial x_i} + \rho g_i + F_i + \frac{\partial}{\partial x_j}\left(\overline{\rho u_i' u_j'}\right) \tag{2}$$

The equation for the turbulence kinetic energy k:

$$\frac{\partial}{\partial t}(\rho k) + \frac{\partial}{\partial x_i}(\rho k u_i) = \frac{\partial}{\partial x_i}\left[\left(\mu + \frac{\mu_t}{\sigma_k}\right)\frac{\partial k}{\partial x_j}\right] + G_k - \rho\varepsilon_k \tag{3}$$

And, the equation for the turbulence dissipation rate ε:

$$\frac{\partial}{\partial t}(\rho\varepsilon) + \frac{\partial}{\partial x_i}(\rho\varepsilon u_i) = \frac{\partial}{\partial x_i}\left[\left(\mu + \frac{\mu_t}{\sigma_k}\right)\frac{\partial \varepsilon}{\partial x_j}\right] + G_{1\varepsilon}\frac{\varepsilon}{k}G_\varepsilon + G_{2\varepsilon}\rho\frac{\varepsilon^2}{k} \tag{4}$$

In these equations u is the velocity, subscripts i and j are 1, 2 or 3 representing x, y or z components, respectively. μ is the dynamic viscosity of water. G_k is the generated turbulence kinetic energy due to the mean velocity gradients, and $G_{1\varepsilon}$ and $G_{2\varepsilon}$ are constants.

To close the system of equations, the turbulent viscosity μ_t is introduced to replace the last term of equation (2), which is given by [14]:

$$\mu_t = \rho C_\mu \frac{k^2}{\varepsilon} \tag{5}$$

where $C_\mu = 0.09$, $G_{1\varepsilon} = 1.44$, $G_{2\varepsilon} = 1.92$, $\sigma_k = 1.0$ and $\sigma_\varepsilon = 1.3$.

3. Results and discussion

3.1 Validation of numerical framework

Due to the very limited availability of experimental and simulation data for microbubble based drag reduction, the present numerical framework is only validated by simulating the no-bubble water flow around the bare hull DARPA SUBOFF, for which the experimental data can be obtained. The main particulars of the DARPA SUBOFF used are specified in Table 1 [15-16].

Table 1 Main particulars of bare hull DARPA SUBOFF submarine

Description	Symbol	Magnitude	Unit
Length of overall	L	4.356	m
Length between perpendiculars	L_{pp}	4.261	m
Maximum hull radius	R_{max}	0.254	m
Centre of buoyancy (aft of nose)	FB	0.4621L	-
Volume of displacement	∇	0.708	m^3

	Wetted surface	S_{wa}	5.998	m^2

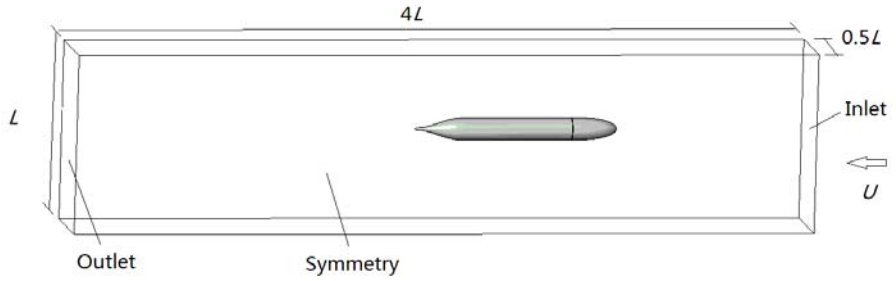

Fig. 1 Computational domain and boundary conditions for the SUBOFF model

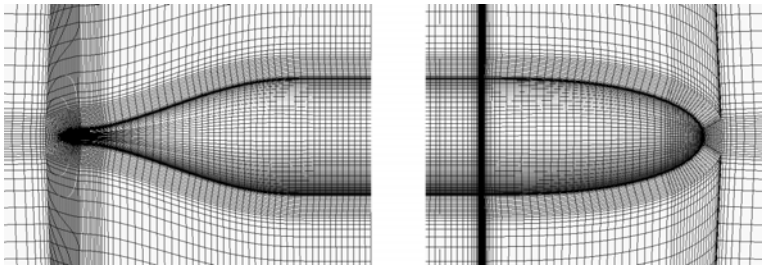

Fig. 2 Mesh on the fore body and aft body of the SUBOFF model

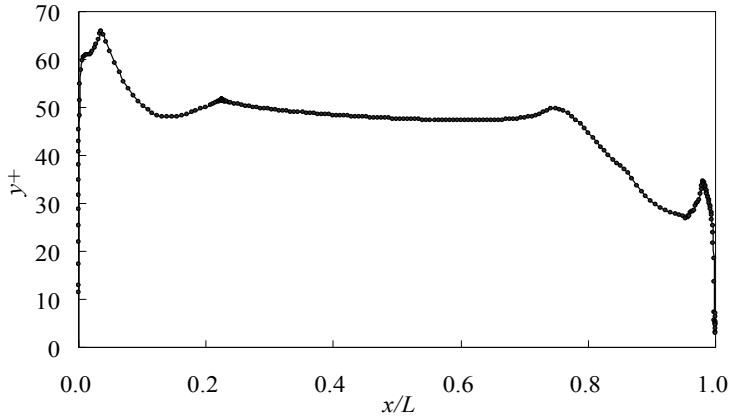

Fig. 3 Distribution of y+ values along the hull of the SUBOFF model at U=3.34 m/s

Since the SUBOFF model has a symmetry plane, only a half of the hull is considered in the simulation. As shown in Fig. 1, the inflow plane is located about L before the hull and the outflow $2L$ after the hull. The width and height of the computational domain are $0.5L$ and L, respectively. Hexahedral meshes containing approximately 1.1 million cells are constructed using ANSYS ICEM. Fig. 2 shows the details of the mesh around the fore and aft bodies of the SUBOFF model. The y+ value, defined as the non-dimensional wall-normal distance of the center of the first cell from the wall, has been checked along the length of the SUBOFF model after each simulation. As an example, the distribution of y+ for one case at freestream velocity of 3.34 m/s is shown in Fig. 3. It is shown that most of the y+ values fall between 30 and 70, which satisfies the 30~100 requirement for the standard wall functions. The inspection results indicate that the present turbulence simulations are trustworthy.

These results are compared against the experimental data from Crook [17] and Huang et al.[18]. Fig. 4 shows that the resistance predicted by the CFD simulations is very close to the experimental data and the simulations show pretty good predictions at a wide range of water speeds. Also as shown in Figs. 5 and 6, although slight discrepancies at the bow and stern

areas appear, the predictions of the friction and pressure coefficients are generally in good agreements with the experiment data.

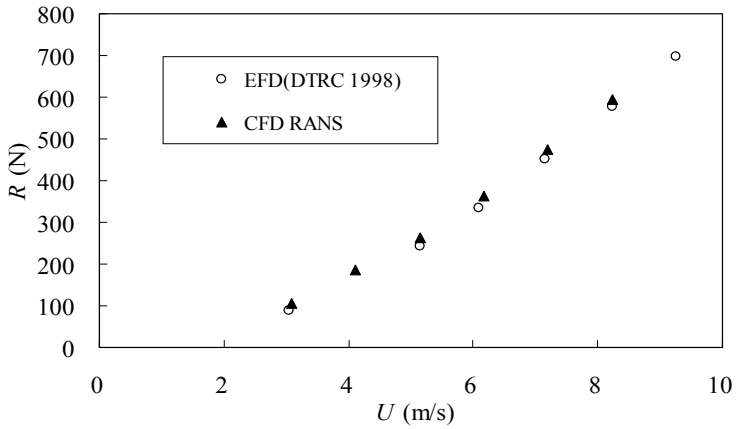

Fig. 4 Resistance of SUBOFF Model 5470

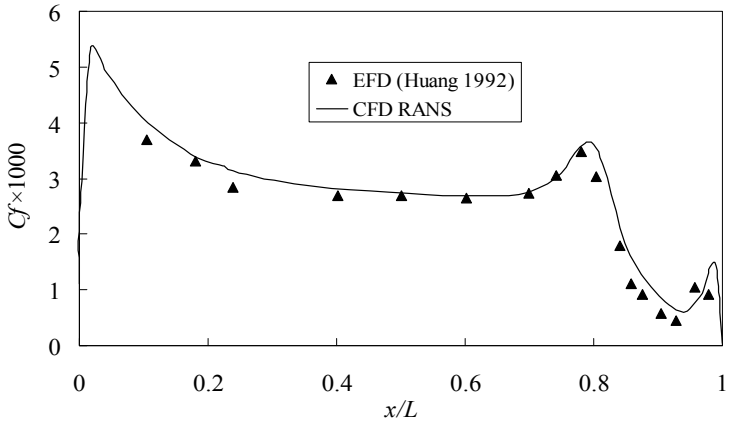

Fig. 5 Friction coefficients along the hull at U=3.34 m/s

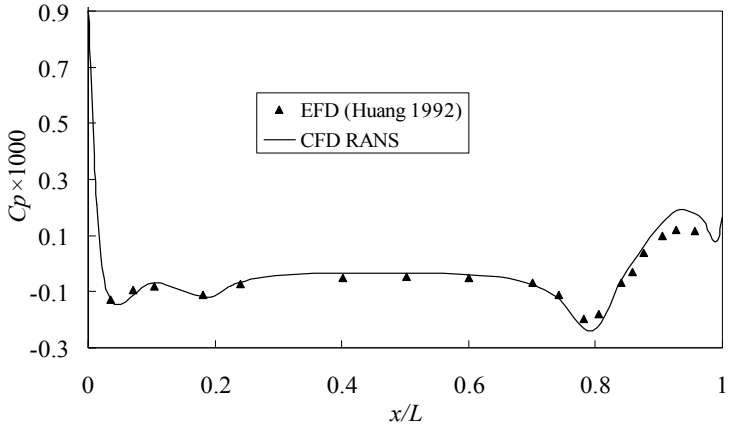

Fig. 6 Pressure coefficients along the hull at U=3.34 m/s

3.2 Effects of velocity ratio V_r and air volume fraction α

On the present SUBOFF model, air bubbles are issued circumferentially from a slot of 10mm width at the bow-body joint (x/L=0.233). Simulations are conducted to investigate the effects of velocity ratio V_r and air volume fraction α with water velocities of 3m/s, 8m/s and

15m/s, which correspond to the Reynolds numbers $Re = 1.30\times10^7$, 3.47×10^7 and 6.50×10^7, respectively.

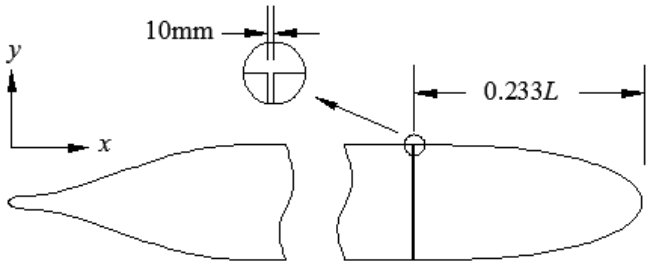

Fig. 7 Injection of air bubbles from the SUBOFF model

The velocity ratio V_r is defined as

$$V_r = \frac{U_a}{U_w} \tag{6}$$

where U_a is injection velocity of microbubbles and U_w is the water velocity.

The resistance reduction rate is defined as

$$\eta = \frac{R - R_0}{R_0} \times 100\% \tag{7}$$

where R denotes resistance with microbubbles and R_0 without microbubbles. For friction resistance, pressure resistance and total resistance, reduction rates η_t, η_f and η_p can be defined respectively. As indicated in equation (7), $\eta < 0$ denotes resistance decreases while $\eta > 0$ means that resistance gets an increase.

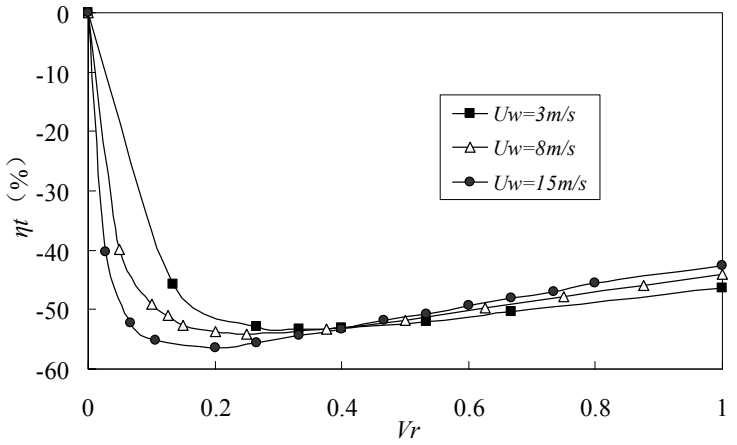

Fig. 8 Reduction rates of total resistance against velocity ratio at different water velocities

As shown in Fig. 8, the total resistance of the SUBOFF model with microbubble can be reduced as much as 55% at the velocity ratio of $V_r = 0.2$ and water velocity of $U_w = 15\text{m/s}$. It first increases and then decreases as the increase of velocity ratio, and the peak of reduction is at velocity ratios of about $V_r = 0.2 \sim 0.3$ for different water velocities.

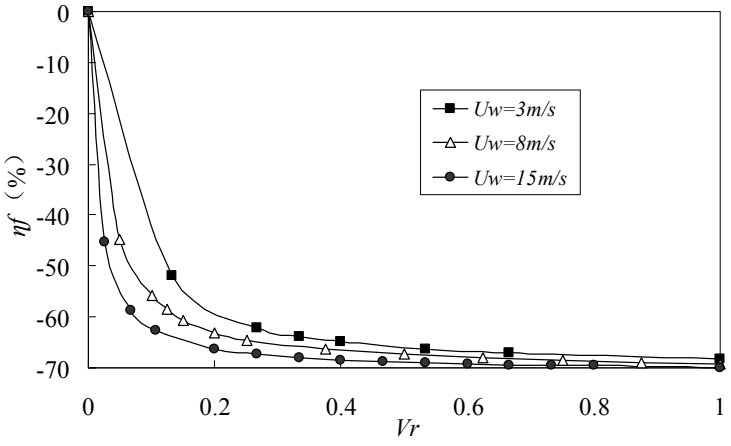

Fig. 9 Reduction rate of friction resistance against velocity ration at different water velocities

As shown in Fig. 9, the reduction of friction resistance increases as the increase of velocity ratio, and the maximum reduction is about 70%. In addition, the change of the reduction decreases as velocity ratio increases. The reduction becomes almost constant when V_r is close to 1. It's also found that higher water speeds result in higher reduction of the friction resistance. The variation of pressure resistance shown in Fig. 10 reveals that, air injection leads to the increase of pressure resistance at various water velocities in the present study, with the exception in the region of $V_r < 0.2$ though.

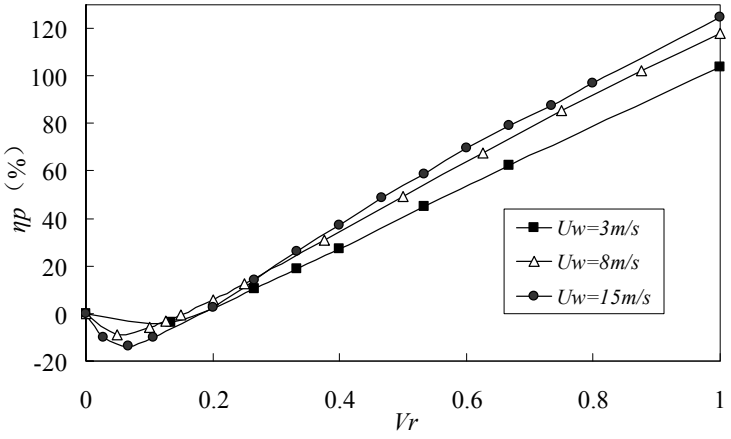

Fig. 10 Reduction rate of pressure resistance against velocity ratio at different water velocities

The influence of air volume fraction α on friction resistance reduction η_f is studied at the water speed of $U_w = 8\text{m/s}$. Fig. 11 shows the profiles of α along the wall-normal distance (h/R_{max}) at a station of the hull stern, under different velocity ratios. Obvious decrease of air volume fraction with increasing the wall-normal distance is observed. The near-wall gradient of air volume fraction profiles for cases of low velocity ratios ($V_r \le 0.2$) is so high that there is little air in the flow at a wall-normal distance of only h/R_{max}=0.05. Fig. 11 also shows that for a given wall-normal distance, the higher the velocity ratio, the higher the air volume fraction.

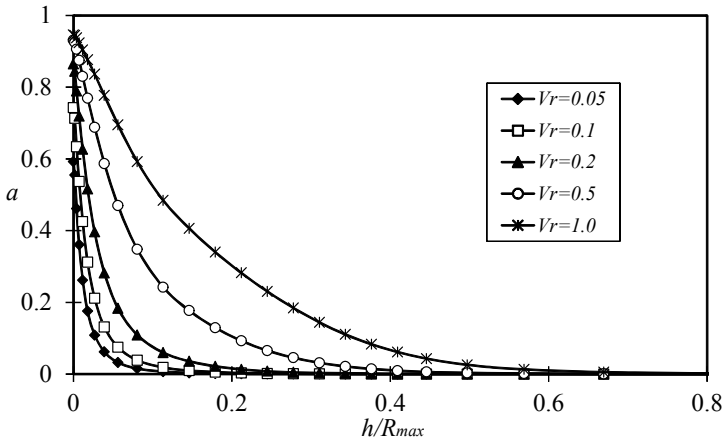

Fig. 11 Air volume fraction profiles at a certain vertical profile above the hull stern (x/L=0.92)

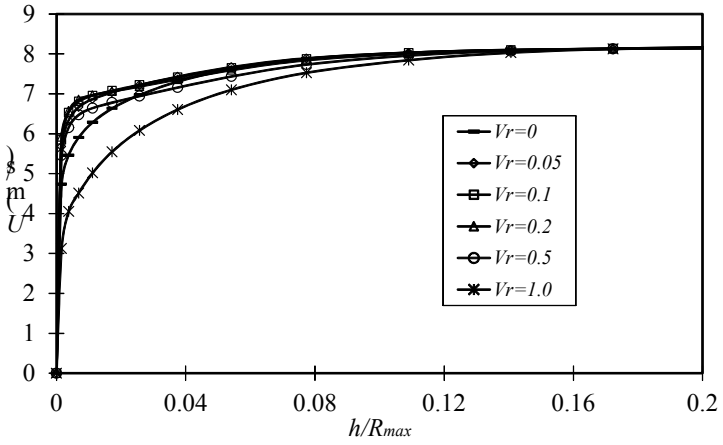

Fig. 12 Velocity profiles along wall-normal direction above the air inlet (x/L=0.233)

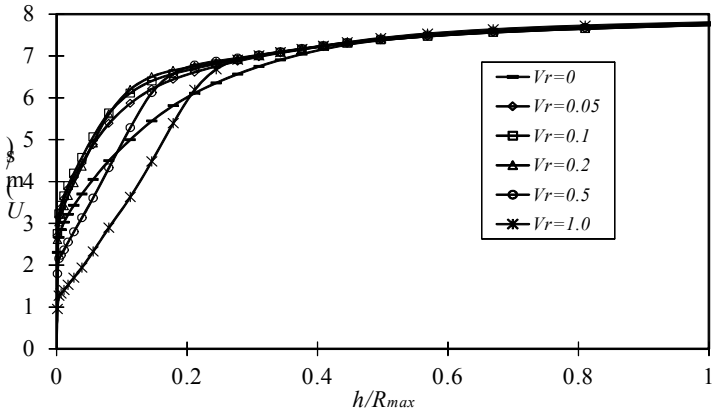

Fig. 13 Velocity profiles along wall-normal direction at a station of the hull stern (x/L=0.92)

The effects of velocity ratio on the velocity profiles at two streamwise stations are shown in Fig. 12 (x/L=0.233) and Fig. 13 (x/L=0.92). As seen from the figures, the velocity profiles with air almost concentrate at distances of h/R_{max}=0.1 over the air inlet (x/L=0.233) and h/R_{max}=0.3 for hull stern profile (x/L=0.92). Lower velocity ratio results in higher velocity gradients in the near-wall boundary layer, with the exception of zero velocity ratio.

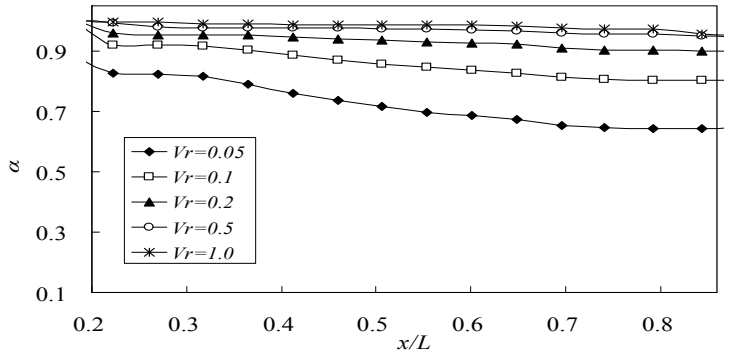

Fig. 14 Distribution of air volume fraction alone the hull at different velocity ratios

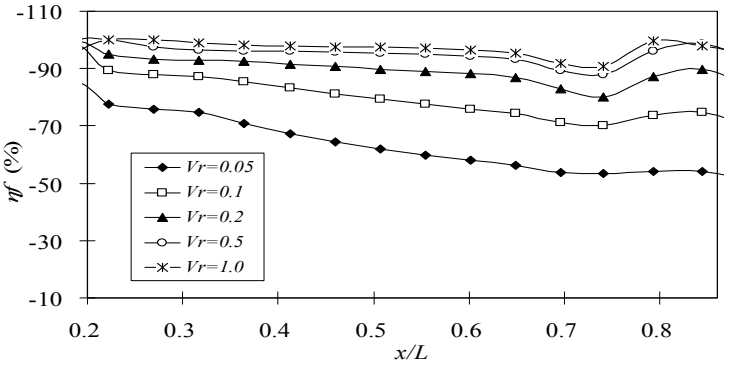

Fig. 15 Distribution of reduction rate of friction resistance alone the hull at different velocity ratios

The air volume fraction and friction resistance reduction alone the hull at different velocity ratios are shown in Figs. 14 and 15, respectively. It is found that the variation of reduction rate of friction resistance alone the mid body of the SUBOFF model ($0.233<x/L<0.745$) follows the same trend as that of the air volume fraction. Both of them gradually decrease along the flow direction. In addition, as shown in these two figures, higher velocity ratio leads to higher air volume fraction and higher friction resistance reduction rate.

4. Conclusions

The CFD mixture model is applied to study the effects of air-injection-to-freestream velocity ratio and air volume fraction on microbubble resistance reduction on a SUBOFF model. After the numerical framework is validated, the study on the effect of velocity ratio to resistance reduction is conducted. Results show that the total resistance reduction of the SUBOFF model with microbubble increases first and then decrease as the increase of velocity ratio. The peak of the reduction that is approximately equal to 55% is at the velocity ratio of about $V_r = 0.2 \sim 0.3$. However, the reduction of the friction resistance increases with the increase of velocity ratio, and the reduction rate becomes almost constant when the velocity ratio is close to 1. Both the reduction gradients of the total resistance and of the friction resistance at $V_r < 0.2$ are much higher than those at $V_r > 0.3$ (shown in Fig. 8 and 9). The variations of both the velocity profiles and air volume fraction profiles indicate that microbubbles of different velocity ratios are able to change the boundary layer flow and result in different resistance performance for the SUBOFF model. Since the variations of the friction resistance reduction and of air volume fraction alone the mid body of the SUBOFF model share similar trends, it is concluded that the near-wall air volume friction play an important role in friction resistance reduction.

REFERENCES

[1] XU, J., MAXEY, M. R., KARNIADAKIS, G. E.: "*Numerical simulation of turbulent drag reduction using micro-bubbles*", Journal of Fluid Mechanics 468 (2002) p. 271-281.

[2] KIM, S., CLEAVER, J. W.: "*The persistence of drag reduction following the injection of microbubbles into a turbulent boundary layer*", International Communications in Heat and Mass Transfer 22 (1995) p. 353-357.

[3] BONDELIND, M., SASIC, S., KOSTOGLOU, M., BERGDAHL, L., PETTERSSON, T. J. R.: "*Single- and two-phase numerical models of Dissolved Air Flotation: Comparison of 2D and 3D simulations*", Colloids and Surfaces A: Physicochemical and Engineering Aspects 365 (2010) p. 137-144.

[4] KUNZ, R. F., GIBELING, H. J., MAXEY, M. R., TRYGGVASON, G., FONTAINE, A. A., PETRIE, H. L., CECCIO, S. L.: "*Validation of Two-Fluid Eulerian CFD Modeling for Microbubble Drag Reduction Across a Wide Range of Reynolds Numbers*", Journal of Fluids Engineering 129 (2007) p. 66-79.

[5] MOHANARANGAM, K., CHEUNG, C. P., TU, J. Y., CHEN, L.: "*Skin friction reduction by introduction of micro-bubbles into turbulent boundary layer*", Proceedings of the 16th Australasian Fluid Mechanics Conference, Gold Coast, Australia, 2007.

[6] KANAI, A., MIYATA, H.: "*Direct numerical simulation of wall turbulent flows with microbubbles*", International Journal for Numerical Methods in Fluids 35 (2001) p. 593-615.

[7] LATORRE, R.: "*Ship hull drag reduction using bottom air injection*", Ocean Engineering 24 (1997) p. 161-175.

[8] MOHANARANGAM, K., CHEUNG, S. C. P., TU, J. Y., CHEN, L.: "*Numerical simulation of micro-bubble drag reduction using population balance model*", Ocean Engineering 36 (2009) p. 863-872.

[9] MADAVAN, N. K., DEUTSCH, S., MERKLE, C. L.: "*Reduction of turbulent skin friction by micro-bubbles*", Physics of Fluids 27 (1984).

[10] DOĞRUL, A., ARıKAN, Y., ÇELIK, F.: "*A numerical investigation of air lubrication effect on ship resistance*", International Conference on Ship Drag Reduction, Istanbul, Turkey, 2010.

[11] SKUDARNOV, P. V., LIN, C. X.: "*Drag reduction by gas injection into turbulent boundary layer: Density ratio effect*", International Journal of Heat and Fluid Flow 27 (2006) p. 436-444.

[12] CECCIO, S. L.: "*Friction drag reduction of external flows with bubble and gas injection*", Annual Review of Fluid Mechanics 42 (2010) p. 183-203.

[13] SANDERS, W. C., WINKEL, E. S., DOWLING, D. R., PERLIN, M., CECCIO, S. L.: "*Bubble friction drag reduction in a high-Reynolds-number flat-plate turbulent boundary layer*", Journal of Fluid Mechanics 552 (2006) p. 353-380.

[14] YAN, X., LIU, J., CAO, Y., WANG, L.: "*A single-phase turbulent flow numerical simulation of a cyclonic-static micro bubble flotation column*", International Journal of Mining Science and Technology 22 (2012) p. 95-100.

[15] GROVES, N. C., HUANG, T. T., CHANG, M. S.: "*Geometric characteristics of DARPA SUBOFF models (DTRC Model Nos. 5470 and 5471)*", Report No. DTRC/SHD-1298-01 (1989).

[16] TOXOPEUS, S.: "*Viscous-flow calculations for bare hull DARPA SUBOFF submarine at incidence*", International Shipbuilding Progress 55 (2008) p. 227-251.

[17] CROOK, B.: "*Resistance for DARPA SUBOFF as Represented by Model 5470*", David Taylor Research Center report DTRC/SHD-1298-07 (1990).

[18] HUANG, T., LIU, H. L., GROVES, N., FORLINI, T., BLANTON, J., GOWING, S.: "*Measurements of flows over an axisymmetric body with various appendages in a wind tunnel: the DARPA SUBOFF experimental program*", 19th Symposium on Naval Hydrodynamics, Seoul, South Korea, 1992.

Submitted: 29.03.2013.
Accepted: 06.06.2014.

Xujian Lyu [1], Hui Tang [1a], Jianglong Sun [2], Xiaoguang Wu [2], Xianwen Chen [3]
[1] School of Mechanical and Aerospace Engineering
Nanyang Technological University, Singapore 639798
[2] School of Naval Architecture and Ocean Engineering,
Huazhong University of Science and Technology, Wuhan 430074, China
[3] Wuchang Shipbuilding Industry Company Ltd.,
Wuhan 430060, China
[a] Author for correspondence: htang@ntu.edu.sg